Article

Red Mud-Reduced Graphene Oxide Nanocomposites for the Electrochemical Sensing of Arsenic

Sujit Deshmukh, Debosmita Banerjee, Gourav Bhattacharya, Sam J. Fishlock, Anjan Barman, James A. McLaughlin, and Susanta Sinha Roy

ACS Appl. Nano Mater., **Just Accepted Manuscript** • DOI: 10.1021/acsanm.0c00165 • Publication Date (Web): 10 Apr 2020

Red Mud-Reduced Graphene Oxide Nanocomposites for the Electrochemical Sensing of Arsenic

Sujit Deshmukh[†], Debosmita Banerjee[†], Gourav Bhattacharya[‡], Sam J. Fishlock[‡], Anjan Barman[§], James McLaughlin[‡], Susanta Sinha Roy[†*]

[†]Department of Physics, School of Natural Sciences, Shiv Nadar University, NH-91, Uttar Pradesh 201314, India.

[‡]Nanotechnology and Integrated Bioengineering Centre, University of Ulster, Jordanstown Campus, Newtownabbey, BT37 0QB, Northern Ireland, UK.

[§]Department of Condensed Matter Physics and Material Sciences, S. N. Bose National Centre, Block JD, Sector III, Salt Lake, Kolkata 700098, India.

ABSTRACT

This work demonstrates the applicability of red mud-reduced graphene oxide (RM-rGO) nanocomposites, for the reliable and selective electrochemical detection of arsenic. The new nanocomposite material shows excellent anti-interference activity towards the arsenic ions (As^{3+}) with the co-occurrence of other common cations (Cd^{2+}, Cr^{2+}, Zn^{2+}, Pb^{2+}, and Hg^{2+}). Especially, the nanocomposite is exceptionally selective for As^{3+} in the presence of Cu^{2+} ions, which is stated to be the main interfering agent in the electrochemical detection of As^{3+}. Under optimal experimental conditions, the new nanocomposite displays a high sensitivity (2.49 μA/ppb) as well as a very low detection limit (0.07 ppb) towards As^{3+} detection. This excellent electrochemical performance of the composite is accounted for the high adsorption proficiency of hematite (Fe_2O_3) phase rich nano red mud particles and enhanced electron transfer kinetics due to the presence of rGO.

KEYWORDS: Red mud, arsenic, hematite, electrochemical detection, sensitivity, electron transfer kinetics.

INTRODUCTION

Arsenic ion (As^{3+}), a highly toxic substance, widely distributed in nature and one of the most abundant mineral in the earth's crust.[12] According to the World Health Organization (WHO), the maximum acceptable level of As^{3+} in drinking water is 10 ppb and around 20 countries are suffering from serious As^{3+} contamination.[3] The determination of trace level (sub ppb) of As^{3+} in natural water (ocean, sea, rivers), wastewater (from mining, metal processing, pesticides, organic

chemicals, etc.) and drinking water has become very important because these media are vulnerable to As^{3+} contamination.[4] Among many developed methods for toxic metal ions detection,[5,6] electrochemical (EC) techniques especially, low-cost stripping voltammetry has gained considerable interest in terms of sensitivity, portability, rapid analysis time and suitable for on-site detection.[7,8] The performance of such methods, however, depends heavily on the materials used for detection purposes.

Over the decades metal oxide nanoparticles (NPs) with their strong adsorption ability or electrocatalytic activity against toxic metal ions were explored to improve the EC sensor technology.[9–12] However, owing to the electrode fouling and inferior electrical conductivity, most of the metal oxide NPs suffer from long-term stability and unfavorable electron transfer kinetics.[13] On the other hand, graphene and its associates (graphene oxide/reduced graphene oxide) have gained significant attention in the field of electrochemistry, due to their tunable electrical conductivity, high electron mobility, and large surface area.[14–16] The combination of graphene with metal oxide NPs can, therefore, overcome the drawbacks present in the metal oxides and can provide a modern EC platform for the detection of toxic metal ions. Up to now Fe_3O_4, Fe_2O_3, MnO_2, PbO based graphene nanocomposites(NCs) have been utilized with great success for As^{3+} detection.[17–19] Among these metal oxides, environmental friendly Fe_3O_4/Fe_2O_3 NPs or nanosheets have shown a higher affinity towards As^{3+}.[7] But sophisticated synthesis protocols of such NCs lead to an increase in the material production cost. Therefore, a facile approach to prepare low-cost NCs, consist of graphene and many metal oxide phases could be of great significance in the field of EC sensor.

Red mud (RM) is an aluminum industry waste, composed of fine particles containing Fe_2O_3 (30-60%) constitutes; in addition, other metal oxides like Al_2O_3, SiO_2, TiO_2 are also present.[20] It possesses large surface areas and available at large scale at practically no cost. However, it is highly alkaline in nature and now is a threat to the ecosystem due to the high volume of RM production, processing, and maintenance. RM is well known to have high adsorption capacity towards toxic metal ions and it has been used for the removal of these environmental carcinogens for decades.[21] Interestingly, the applicability of red mud as an EC sensor towards toxic metal ion detection has not been explored yet.

Thus motivated by the need for a cost-effective, robust, environmental friendly sensor for As^{3+} detection in water and to utilize the excellent adsorption capabilities of RM, herein we report the applicability of RM-reduced graphene oxide (RM-rGO) NCs for As^{3+} detection using square wave anodic stripping voltammetry (SWASV) technique. The evaluation of EC studies of the new NCs exhibit excellent limit of detection (LOD), sensitivity and anti-interference activity towards As^{3+} ions.

EXPERIMENTAL SECTION

RM was collected from National Aluminum Company Limited (NALCO), India. All chemicals including, graphite flakes (>99% Alfa Aesar), sulphuric acid (98%, Fisher Scientific) and hydrochloric acid (37%, Fisher Scientific), potassium permanganate (>99%, Sigma Aldrich), sodium hydroxide (98%, Fisher Scientific), L-ascorbic acid (99%, Sigma Aldrich), potassium ferrocyanide ($K_4[Fe(CN)_6]$), potassium ferricyanide ($K_3[Fe(CN)_6]$), potassium chloride (KCl) (Fisher Scientific) were used as received without any further purification. A stock solution (1 g/L) of As^{3+} was prepared by dissolving the required quantity of As_2O_3 in NaOH solution, and subsequently, the pH of the solution was adjusted to 3 with concentrated HCl. For interference study, the standard solutions of Cd^{2+}, Cr^{2+}, Zn^{2+}, Cu^{2+}, Pb^{2+}, Hg^{2+} ions (1000 ppm each) were purchased from Sigma Aldrich and were diluted to make a solution of the desired concentration.

First, rGO was synthesized using sonication assisted oxidation of graphite in an acidic environment as reported by Sina Abdolhosseinzadeh et al.[22] In order to prepare the nano RM-rGO composite, mechanical milling process using a planetary ball mill (Retsch, PM200) was employed. The powders (mass ratio of RM to rGO is 10:1) were placed in a chrome steel bowl (volume 60 mL) filled with steel balls of diameter 5 mm with balls-to-powder mass ratio was 10:1. The ball milling was carried out at 150 revolutions per minute (rpm) and was continued up to 12 hr. with intermediate intervals of 2 hr. The prepared samples are designated as RM-rGO_Z NCs where Z is the milling hour.

X-ray diffraction (XRD) experiments were performed using Bruker, D8-discover with Cu-K_α energy (λ = 0.154 nm). The Raman spectra were recorded using a Renishaw Raman spectrometer (inVia) using a 532 nm Laser source, using a nominal power of 25 mW for 60 s, 50× magnification. Fourier transform infrared spectroscopy was performed using Thermo Scientific Nicolet™iS™5 FTIR with a diamond ATR accessory. Scanning electron microscopy was carried out using a Hitachi SU5000, with an acceleration voltage of 10 kV and working distance □ 6 mm. All EC

measurements were done using the Autolab potentiostat/galvanostat 302N instrument (Metrohm Autolab B.V. Utrecht, Netherlands) controlled by NOVA software.

RESULTS AND DISCUSSION

Morphology of the RM, rGO and RM-rGOz NCs can be visualized in SEM images (Figure 1). In case of rGO, an aggregated and crumpled paper-like structure is observed in Figure 1a, which is a common characteristic of oxidation/reduction processed rGO.[22] Whereas, RM particles (Figure 1b) are expressing their characteristics feature of irregular size and shape with particle sizes are ranging from 3 to 5 μm. while their agglomerates are distributed within tens of micrometer range. Figure 1(c-e) shows clear changes in the morphology in the RM-rGO NCs caused by ball milling. During the first four hours of ball milling cold welding and cracking mechanism together participate in the formation of spherical size particles.[23] Increasing milling time increases structural disorder, decreases particle size and peel off graphene layers. After 8 hours of milling period, considerable refinement and reduction in particle size is evident. With further increasing the milling time, the particles are being fragmented into more tiny particles and particles tend to agglomerate again. This simple and facile strategy to prepare NPs from particles of micron size has a direct impact on their EC performances, which is discussed next.

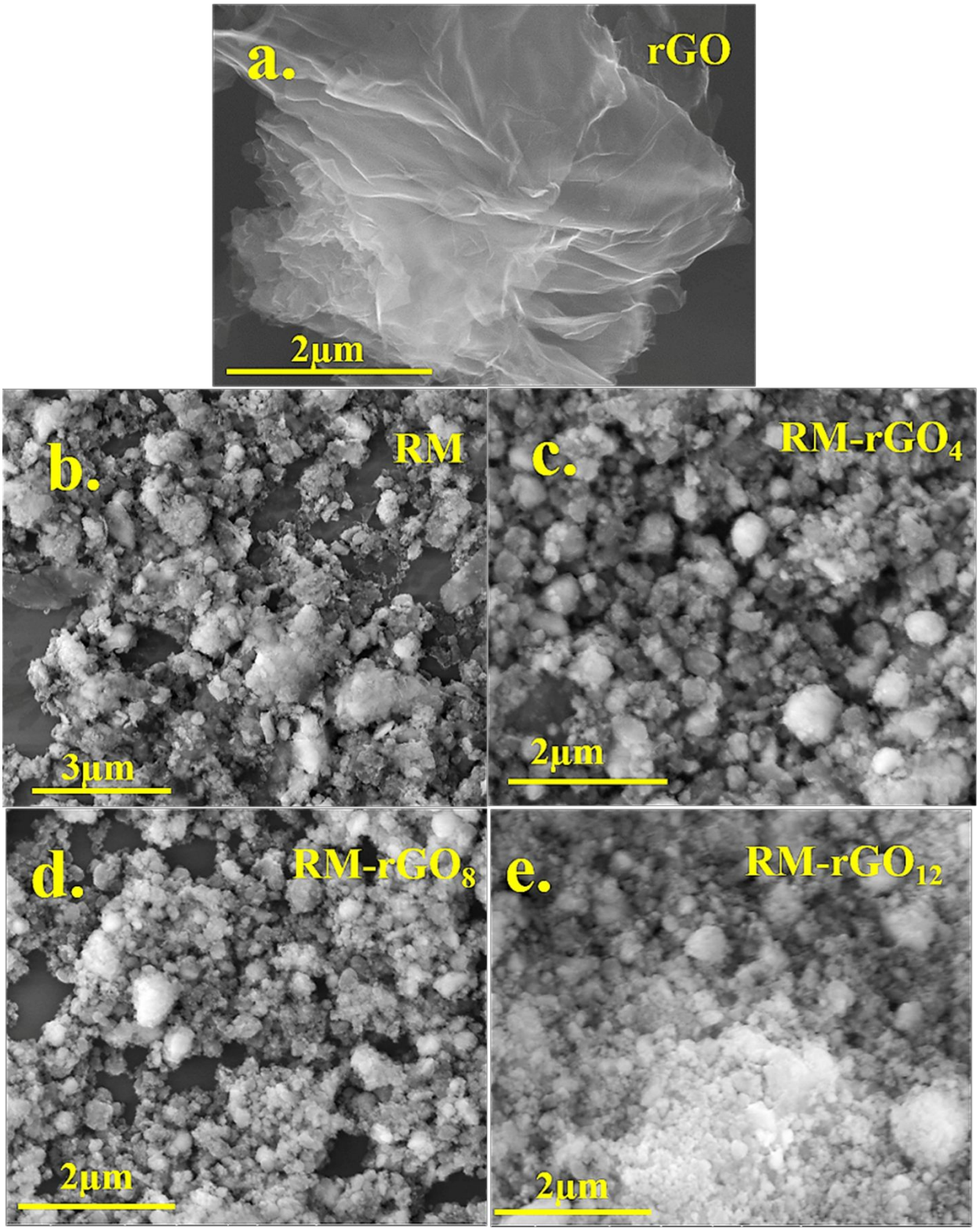

Figure 1 SEM images of (a) rGO (b) RM (c) RM-rGO_4 (d) RM-rGO_8 and (e) RM-rGO_{12}.

In order to investigate the charge transfer kinetics of the prepared NCs, cyclic voltammetry (CV) measurements were performed using an EC redox couple ($[Fe(CN)_6]^{3-/4-}$ in 0.1M KCl), which is displayed in Figure 2a. It is well known that both the degree of reversibility and the charge transfer kinetics, can be improved by eliminating oxygen-containing groups or by increasing the fraction of sp^2 bonded carbons in carbon-based NCs.[24] In our case, the smallest ΔE_p □ 0.15 V (anodic and cathodic peak potential separation) and the highest peak current is observed for RM/rGO$_8$ NCs. Further, the ratio of anodic to cathodic peak current (i_{pa}/i_{pc}) is calculated as 1.08 for RM/rGO$_8$, indicating a reversible electron transfer process of the Fe^{2+}/Fe^{3+} species. The CV output of RM/rGO$_{12}$ is also comparable to that of RM/rGO$_8$. From the scan rate dependency CV curves of RM/rGO$_8$ (inset of Figure 2a), it can be visualized that redox peak currents (i_{pa} and i_{pc}) are increases linearly with the square root of scan rate (insets of Figure 2a), implies diffusion-controlled redox kinetics of the Fe^{2+}/Fe^{3+} species. The CV performance of RM-rGO$_2$, RM-rGO$_6$, and RM-rGO$_{10}$ is also represented in Figure S1. The CV output of RM-rGO$_6$ and RM-rGO$_{10}$ are approximately equal to that of RM-rGO$_4$ and RM-rGO$_{12}$ respectively whereas, the lowest peak current is observed for RM-rGO$_2$.

Figure 2b represents the SWASV analytical characteristics of GCE, RM and all RM-rGO NCs where electrodeposition is carried out for 200 s at -0.4 V. Nearly no oxidation peak is observed for the bare GCE electrode. For RM particles there is only a weak peak can be seen. This is probably due to the inferior electrical conductivity of the RM. However, the RM-rGO NCs provide a much greater and sharper peak current response towards the As^{3+} ions. Figure 2b clearly shows that RM-rGO$_8$ outperforms the other electrodes in terms of stripping peak current response corresponds to the oxidation of As^0. RM-rGO$_8$ is, therefore, best suited for As^{3+} detection which results in better sensitivity.

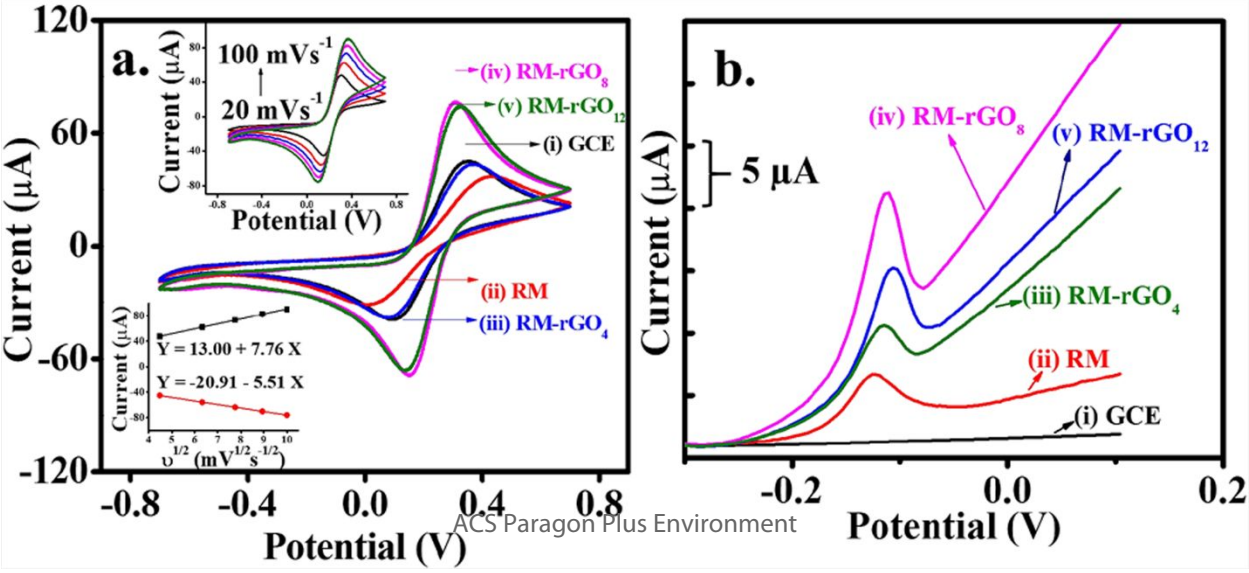

Figure 2 (a) CV response of (i) GCE (ii) RM (iii) RM-rGO_4 (iv) RM-rGO_8 and (v) RM-rGO_{12} with insets showing the CV response of RM-rGO_8 with scan rate 20, 40, 60, 80 and 100 mVs^{-1} and the variation of the anodic and cathodic peak current of RM-rGO_8 as a function of scan rate. (b) SWASV response of (i) GCE (ii) RM (iii) RM-rGO_4 (iv) RM-rGO_8 and (v) RM-rGO_{12} for the detection of 10 ppb As^{3+} ions. The SWASV experimental parameters are as follows: deposition time 200 s, deposition potential -0.4 V, amplitude 25 mV, step potential 4 mV and frequency 25 Hz.

Next, experimental parameters (deposition potential and time) of SWASV experiment are optimized (Figure S2) to achieve the maximum sensing efficiency using RM-rGO_8 NCs. Finally, the detection of As^{3+} is accomplished under the optimized experimental conditions (deposition potential of -0.4 V and deposition time 200 s). Figure 3a represents the SWASV response for As^{3+} at various concentrations. The electrooxidation current was linear within the concentration range of 0.5 to 3.7 ppb (inset of Figure 3a) and the fitted linear relationship between the stripping peak current (corresponds to the oxidation of As^0 - As^{3+}) and concentration of As^{3+} is described by the following equation $i/\mu A = -0.59 + 2.49c/ppb$. The limit of detection (LOD) and sensitivity value was found to be 0.07 ppb and 2.49 $\mu A\ ppb^{-1}$ respectively. Where LOD is defined as the, lowest quantity of analyte that provides a signal which is significantly different from the blank value with a stated confidence level of 90% and the LOD value is calculated according to the literature reported.[25] The obtained LOD value is well below the WHO toxicity mark (10 ppb).[3] A comparative study of the performance of the RM-rGO_8/GCE electrode with other sensing platforms developed for EC detection of As^{3+} is summarized in Table 1.

To validate the selectivity of the RM-rGO_8/GCE electrode with the co-occurrence of As^{3+} and Cu^{2+} ions, SWASV measurements were carried out again in a mixture of both the ions where the concentration of Cu^{2+} was kept higher than 8 ppb. Figure 3b represents the SWASV plots of simultaneous detection of As^{3+} and Cu^{2+}. An isolated anodic peak corresponding to the oxidation of Cu^0 – Cu^{2+} is observed at around 0.3 V which is far away (~ 400 mV) from the anodic peak potential of As^0. Here the concentration of As^{3+} and Cu^{2+} is increased simultaneously and the obtained sensitivity of As^{3+} is marginally improved compared to that observed in the absence of Cu^{2+}. The enhanced sensitivity of As^{3+} can be explained on the basis of interference between As^{3+} and Cu^{2+} ions. The stripping peak potentials of both the ions are far from each other (400 mV) and the formation of an intermetallic compound is most unlikely, but small peaks in between As^{3+} and Cu^{2+} are visible which may be due to the formation of As-Cu intermetallic compound during the simultaneous existence arsenic and copper. Such kinds of observations are well documented and

have been published before.[26] The influence of other metal ions on the stripping current response of As^{3+} has been further demonstrated by doing interference experiments.

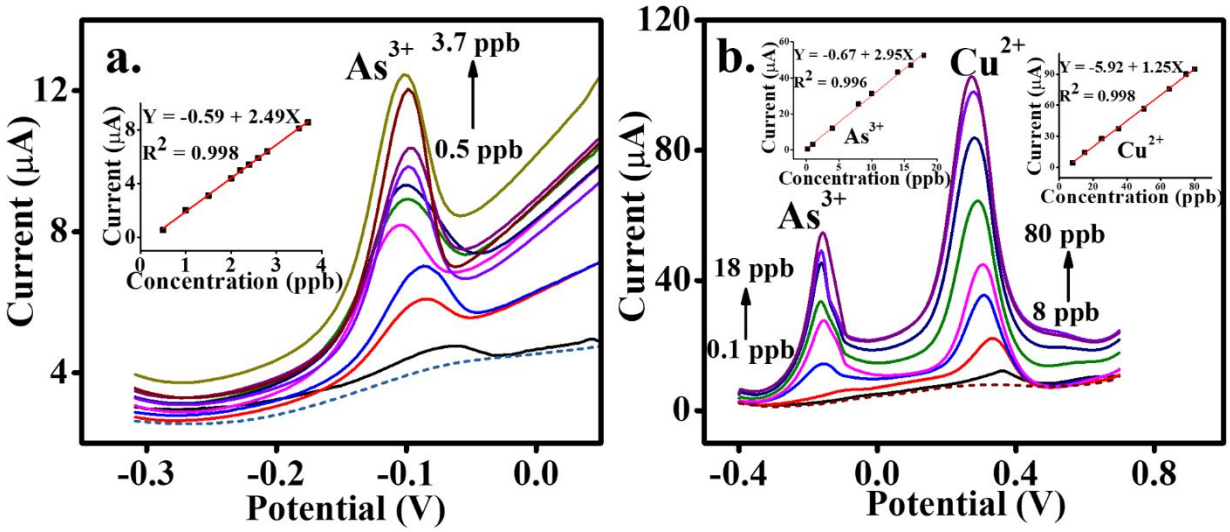

Figure 3 (a) SWASV response of RM-rGO_8 towards the detection of As^{3+} ions over a concentration range of 0.5 to 3.7 ppb. The inset of Figure (a) displays the linear calibration plot of the peak current as a function of As^{3+} ions concentration. (b) SWASV response of RM-rGO_8 for the simultaneous detection of As^{3+} (0.1 to 18 ppb) and Cu^{2+} (8 to 80 ppb) with insets show the linear calibration plots corresponding to the As^{3+} and Cu^{2+} ions concentration.

Table 1. Comparison of our proposed electrode material with other sensing platforms.

Electrode material	Sensitivity (μA/ppb)	LOD (ppb)	Ref.
CoOx/GCE	0.00148	0.825	27
Fe_3O_4 room temperature ionic liquid composite	4.91	0.0008	10
Ru nanoparticle/GCE	0.00238	0.1	28
Gold nanoparticles	2.69	0.06	29
Au-Pd bimetallic nanoparticle	3.9	0.024	30
FePt bimetallic nanoparticle	0.42	0.8	31
MnOx/Au nanoparticle composite	0.193	0.057	9
$MnFe_2O_4$ nanocrystal/gold electrode	0.295	1.95	32
rGO/MnO_2 nanohybrid	0.175	0.05	18
rGO/Fe_3O_4 nanocomposites	0.281	0.12	19
Dumbbell like Au/Fe_3O_4 nanoparticles	9.43	0.02	33
Graphene/PbO composite	-	0.74	17
RM-rGO composite	2.49	0.07	Present work

Analysis of As^{3+} in the presence of other interfering agent is still difficult, as coexisting substances are co-deposited and stripped with As^{3+}. Therefore selective detection of As^{3+} in the presence of other metal ions is also important. In order to investigate the anti-interference ability

of the RM-rGO$_8$/GCE electrode, SWASV measurements are recorded in 10 ppb As^{3+} solution in the presence of a 10 fold higher concentration of other metal ions namely Cd^{2+}, Cr^{2+}, Zn^{2+}, Cu^{2+}, Pb^{2+}, and Hg^{2+}. Figure 4 illustrates the anodic stripping current of the As^{3+} in the absence and presence of the above mentioned interfering metal ions. No significant interference is observed of these ions on the As^{3+} stripping current response. The optimized deposition potential (-0.4 V) eliminates the possible interference from common metal cations.[19] In addition, rapid mass transportation in the electrode surface with a small diffusion layer and high current density could also be responsible for such good anti-interference activity. This interference study laid the foundation for reliable and selective As^{3+} detection in water.

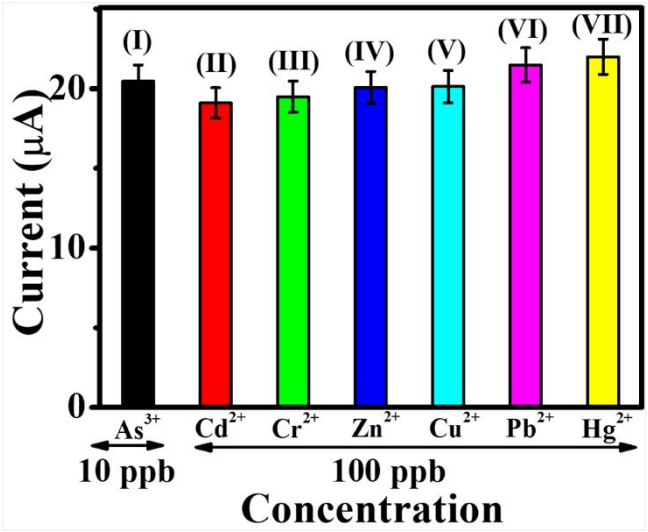

Figure 4 Effect of interfering ions Cd^{2+}, Cr^{2+}, Zn^{2+}, Cu^{2+}, Pb^{2+}, and Hg^{2+} on the stripping current response of 10 ppb As^{3+}.

To demonstrate the compatibility of RM-rGO$_8$ NCs with the Au electrode, similar SWASV tests are conducted on the RM-rGO$_8$ modified Au electrode (RM-rGO$_8$/Au) having a physical size (diameter = 2 mm) equal to GCE. Figure S3 (supporting information) displays the typical SWASV curves for the As^{3+} (0.1 to 2.1 ppb) detection with inset represents the linear calibration plot. Interestingly, the anodic peak corresponds to the oxidation of As^0 - As^{3+} occurs around (0.2 V) which is more positive as compared to the RM-rGO$_8$ modified GCE electrode. The obtained sensitivity and LOD are found to be 4.35 μA ppb^{-1} and 0.08 ppb respectively. Though the RM-rGO$_8$/Au electrode affords better sensitivity compared to RM-rGO$_8$/GCE, it is still prone to

interference from other metal ions, in particular from Cu^{2+} ions, which has a redox potential (around 0.338 V) very near to the oxidation potential of As^0.

Metal oxide nanomaterials are prone to instability under acidic media, hence taking the practical applications into account the reproducibility and stability test of the RM-rGO_8 NCs is carried out in acidic conditions. A series of 6-time repetitive measurements of SWASV response for 2 ppb of As^{3+} is recorded and the results are displayed in Figure S4. The stripping current response of the RM-rGO_8 electrode is highly reproducible with a relative standard deviation of 3.57%. The nanocomposite's stability is also investigated and the SWASV current response corresponds to the arsenic oxidation remaining □90 % of its initial response after 15 days. Therefore, the good electrode stability and reproducibility for repetitive measurements of As^{3+} ions indicate that the nanocomposite possesses great potential for monitoring As^{3+} ions in real samples.

In order to examine the practical application of the present NC (RM-rGO_8), the SWASV experiment has been performed on the real water sample. The sample was collected from the groundwater near Asansol city, West Bengal, India. Prior to the SWASV experiment, the sample was treated with a filter to remove any insoluble contaminants. The water sample was then diluted with concentrated HCl to adjust its pH value to 3 and no further sample treatment was done. The standard addition of As^{3+} is performed to calculate the concentration of As^{3+} in the real sample. The SWASV response and the corresponding calibration plots are shown in Figure S5 and the As^{3+} concentration in the real sample is calculated as 2.24 ppb. To determine the validity of the electrochemical method we discussed, recovery experiments are also performed with the real sample in which a known amount of As^{3+} is added. The obtained recovery is varied between 90% to 110% which indicates the RM-rGO_8 nanocomposite has a great practical application.

There are many factors that can influence the EC behavior of RM-rGO NCs, such as surface morphology, the active surface area for EC reaction, the fraction of sp^2 bonded carbons come in contact with the electrolyte, etc. The optimization of milling time is another aspect that requires further analysis in terms of identifying the morphological, chemical and physical changes. In addition, the shift in the peak current (anodic/i_{pa} and cathodic/i_{pc}) response and peak potential difference (ΔE_p) in the CV *i*-E curve may be correlated to the surface oxygen functionalities and the exposed edge planes of sp^2 bonded carbons. In order to identify the factors responsible for the strong EC sensing results, XRD, Raman and FTIR spectroscopic tools are employed.

To determine the different phases present in the as obtained RM and synthesized RM-rGO NCs, XRD measurements were carried out and are represented in Figure 5a. In case of rGO, a broad diffraction peak around $2\theta \sim 25^{o}$ and a small peak at $2\theta \sim 43^{o}$ can be seen (Figure 5a(i)) which signifies the formation of rGO with less oxygen functionalities.[34] Whereas, in RM and all RM-rGO NCs, a mixture of many metal oxide phases such as hematite, goethite, calcite, and silica can be observed. However, hematite ($\theta\sim 12.06^{o}$, 16.57^{o}, 17.80^{o}) is the main dominant phase in RM which is expected due to the red color of the RM and it constitutes around 55% of the RM.[35] The reduction in particle size via ball milling can also be correlated with the XRD peak broadening with milling hour. Notably, in all RM-rGO NCs, the broad diffraction peak of rGO can be observed, indicating that rGO sheets are attached to the RM particles.

Raman measurements were also carried out to examine the phase purity and different vibrational modes present in the NCs. A series of band related to the different modes of vibration of metal oxides, e.g; Eg (~ 291 and 404 cm^{-1}) and A_{1g} (~223 and 502 cm^{-1}) mode of hematite (Fe_2O_3) phase; E_g^5 (~146 cm^{-1}) and A_G^1 (~662 cm^{-1}) mode of ilmenite ($FeTiO_3$) phase; Eg (~152 cm^{-1}) mode corresponds to the calcite ($CaCO_3$) phase can be seen in the Raman spectrum of RM (Figure 5b(i)).[35] Raman spectrum of rGO and RM-rGO NCs display a typical characteristic peak of D and G band around 1345 and 1595 cm^{-1}, where D peak corresponds to the rGO sheet defects and G peak is related to E_{2g} phonon modes of the sp^2 bonded carbon. The relative intensity ratio of these two bands (I_D/I_G) is a simple way to quantify the degree of disorder present in the graphene sheet. In case of rGO, the ratio of the I_D/I_G is 1.00 and the value is increased to 1.13 for the RM-rGO_8 sample, which implies that the physical force during the milling process introduces defects and disorder to the graphene cluster. Further milling up to 12 hr. did not change much the value of I_D/I_G that indicates, rGO sheets are attached well to the RM particles which help graphene sheets to damage further.

Furthermore, FTIR spectroscopy examines the deoxidation of rGO and the presence of chemical bonds or attached functional groups in RM and RM-rGO NCs. In the case of rGO (Figure 5c(i)), the peak at 1560 cm^{-1} and a weak signal around 1685 cm^{-1} is referred to as the C=C and C=O stretching vibration respectively. However, other oxygen-containing functionalities such as epoxy or alkoxy groups (C-O) are completely absent in rGO which are the common features of graphene oxides FTIR spectra.[36] This observation confirms that most of the oxygen-containing functional groups are removed from the graphene sheet during the reduction process. On the other

hand, RM shows a strong absorption band around 595 cm^{-1} and a weak peak near 1645 cm^{-1} due to the stretching vibration of Fe-O bonds of the hematite phase.[37] In addition, the presence of goethite (~803 cm^{-1}), characteristics bands correspond to the Si-O vibrations (~990 cm^{-1}), presence of CO_3^{2-} (~1420, 866 cm^{-1}) groups are also detected. The positions and absorption bands of RM-rGO NCs (Figure 5c(iii-v)) are nearly similar to that of RM. The rGO sheets are likely anchored to the nano RM particles through carboxylate bonds (Fe-C-O) and the existence of which is confirmed in the FTIR spectra (band around 1580 cm^{-1}) of RM-rGO NCs.[38] The existence of some additional bands in the hydroxyl stretching region (~ 3300-3500 cm^{-1}) can also be seen in RM-rGO NCs. These attached hydroxyl functional groups in the RM-rGO NCs are advantageous for adsorbing toxic metal ions.[13]

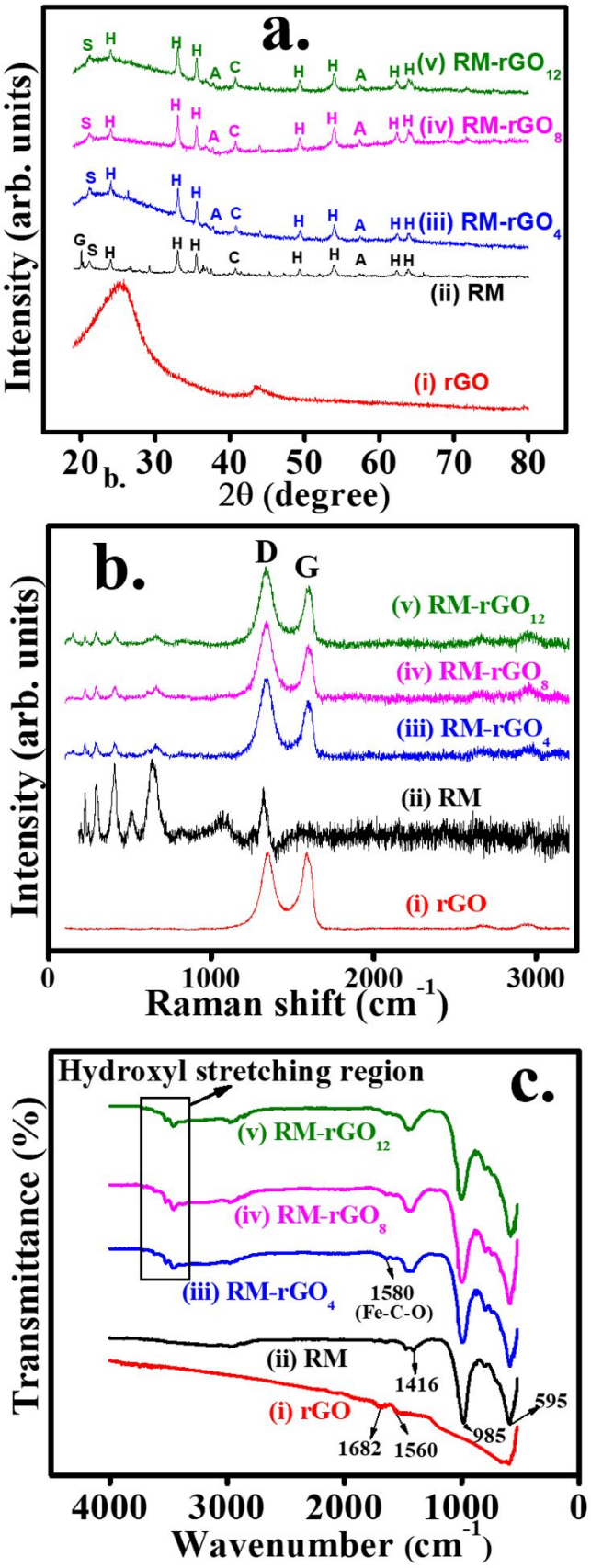
a.
Intensity (arb. units)
(v) RM-rGO12
(iv) RM-rGO8
(iii) RM-rGO4
(ii) RM
(i) rGO
20
30
40
50
60
70
80
2θ (degree)
b.
D
G
Intensity (arb. units)
(v) RM-rGO12
(iv) RM-rGO8
(iii) RM-rGO4
(ii) RM
(i) rGO
0
1000
2000
3000
Raman shift (cm-1)
c.
Hydroxyl stretching region
Transmittance (%)
(v) RM-rGO12
(iv) RM-rGO8
(iii) RM-rGO4
1580
(Fe-C-O)
(ii) RM
1416
(i) rGO
595
985
1682
1560
4000
3000
2000
1000
0
Wavenumber (cm-1)

Figure 5 (a) XRD pattern (b) Raman spectra and (c) FTIR spectra of (i) rGO (ii) RM (iii) RM-rGO_4 (iv) RM-rGO_8 and (v) RM-rGO_{12}.

Thus, the key feature for the excellent EC performance is related to the high adsorption capability of the hematite phase rich RM. The formation of nano RM via mechanical milling increases the active surface area to adsorb As^{3+} ions while the presence of sp^2 bonded carbons in the rGO sheets is responsible for enhanced electron transport kinetics. The superior EC behavior of RM/rGO_8 and RM/rGO_{12} can be attributed to the large active surface area of these NCs where RM particles are properly surrounded by the rGO sheets and larger fraction of sp^2 carbon comes in contact with electrolyte during EC measurements. In addition, the attached functional groups (hydroxyl and carboxylic) to the NC surface not only serve as active sites for electrodeposition of As^{3+} ions but also act as a bridge for rapid electron transfer from solution to electrode surface. Therefore, the NCs prepared at longer milling hour (>4) with exposed sp^2 carbon and less oxygen functionalities facilitates the electron transfer kinetics. The combined effect of RM and electrically conductive rGO allows more effective electrodeposition of As^{3+} ions on the NCs surface, which in turn improves the EC sensing performances.

CONCLUSIONS

In a time of high demand of low-cost potential nanomaterial for environmental carcinogenic detection, this work successfully demonstrates the applicability of mechanically milled RM-rGO NCs as a working electrode material for sensitive and efficient electroanalysis of toxic As^{3+} ions. The electrode (RM-rGO_8) can accurately detect As^{3+} in the presence of other interfering metal ions namely Cd^{2+}, Cr^{2+}, Zn^{2+}, Cu^{2+}, Pb^{2+}, and Hg^{2+}. Mechanical ball milling offers a uniform morphology and enhanced charge transfer kinetics from the low-cost industrial waste RM. However, the optimization of ball milling time is considered to be the key factor to achieve the desirable EC sensing platform. The improvement in the EC performance of RM-rGO NCs with milling time can be attributed to the formation of functionalized RM-rGO NPs which not only provide the large no of active sites for As^{3+} adsorption but also accelerate the electron transport kinetics.

ASSOCIATED CONTENT

Supporting Information

CV response of RM-rGO$_2$, RM-rGO$_4$, RM-rGO$_6$, RM-rGO$_8$, RM-rGO$_{10}$, and RM-rGO$_{12}$ with inset showing the magnified curve of the region A (Figure S1). Experimental parameters optimization (a) deposition potential and (b) deposition time. Other experimental conditions are as follows; amplitude 25 mV, step potential 4 mV and frequency 25 Hz (Figure S2). SWASV response of the RM-rGO$_8$/Au electrode towards the detection of As^{3+} ions over a concentration range from 0.1 to 2.3 ppb. The inset displays the linear calibration plot of the peak current as a function of As^{3+} ions concentration (Figure S3). The reproducibility of 6 times repetitive SWASV measurements of 2 ppb As^{3+} ions using RM-rGO$_8$ nanocomposite modified GCE (Figure S4). SWASV response of real water sample with successive addition of As^{3+} ions. The inset showing the corresponding linear calibration plot of stripping peak current against As^{3+} concentration (Figure S5).

AUTHOR INFORMATION

Corresponding Author

Susanta Sinha Roy - Department of Physics, School of Natural Sciences, Shiv Nadar University, NH-91, Uttar Pradesh 201314, India.

Orcid id- 0000-0001-5078-8877

Email- susanta.roy@snu.edu.in

Authors

Sujit Deshmukh - Department of Physics, School of Natural Sciences, Shiv Nadar University, NH-91, Uttar Pradesh 201314, India.

Orcid id- 0000-0001-7763-1693

Debosmita Banerjee - Department of Physics, School of Natural Sciences, Shiv Nadar University, NH-91, Uttar Pradesh 201314, India.

Orcid id- 0000-0001-5090-257X

Gourav Bhattacharya - Nanotechnology and Integrated Bioengineering Centre, University of Ulster, Jordanstown Campus, Newtownabbey, BT37 0QB, Northern Ireland, UK.

Orcid id- 0000-0001-5235-9240

Sam J. Fishlock - Nanotechnology and Integrated Bioengineering Centre, University of Ulster, Jordanstown Campus, Newtownabbey, BT37 0QB, Northern Ireland, UK.
Orcid id- 0000-0003-0712-8106
Anjan Barman - Department of Condensed Matter Physics and Material Sciences, S. N. Bose National Centre, Block JD, Sector III, Salt Lake, Kolkata 700098, India.
Orcid id- 0000-0002-4106-5658
James McLaughlin - Nanotechnology and Integrated Bioengineering Centre, University of Ulster, Jordanstown Campus, Newtownabbey, BT37 0QB, Northern Ireland, UK.
Orcid id- 0000-0001-6026-8971

CONFLICT OF INTEREST

There are no conflicts to declare

ACKNOWLEDGMENTS

S. Deshmukh and D. Banerjee are indebted to Shiv Nadar University for providing PhD scholarship.

REFERENCES

(1) Clancy, T. M.; Hayes, K. F.; Raskin, L. Arsenic Waste Management: A Critical Review of Testing and Disposal of Arsenic-Bearing Solid Wastes Generated during Arsenic Removal from Drinking Water. *Environ. Sci. Technol.* **2013**, *47* (19), 10799–10812.

(2) Smedley, P. L.; Kinniburgh, D. G. A Review of the Source, Behaviour and Distribution of Arsenic in Natural Waters. *Appl. Geochemistry* **2002**, *17* (5), 517–568.

(3) Aragay, G.; Pons, J.; Merkoçi, A. Recent Trends in Macro-, Micro-, and Nanomaterial-Based Tools and Strategies for Heavy-Metal Detection. *Chem. Rev.* **2011**, *111* (5), 3433–3458.

(4) Nath, P.; Arun, R. K.; Chanda, N. A Paper Based Microfluidic Device for the Detection of Arsenic Using a Gold Nanosensor. *RSC Adv.* **2014**, *4* (103), 59558–59561.

(5) Sengupta, M. K.; Dasgupta, P. K. Oxidation State-Differentiated Measurement of Aqueous Inorganic Arsenic by Continuous Flow Electrochemical Arsine Generation Coupled to Gas-Phase Chemiluminescence Detection. *Anal. Chem.* **2011**, *83* (24), 9378–9383.

(6) Mulvihill, M.; Tao, A.; Benjauthrit, K.; Arnold, J.; Yang, P. Surface-Enhanced Raman Spectroscopy for Trace Arsenic Detection in Contaminated Water. *Angew. Chemie Int. Ed.* **2008**, *47* (34), 6456–6460.

(7) Deshmukh, S.; Kandasamy, G.; Upadhyay, R. K.; Bhattacharya, G.; Banerjee, D.; Maity, D.; Deshusses, M. A.; Roy, S. S. Terephthalic Acid Capped Iron Oxide Nanoparticles for Sensitive Electrochemical Detection of Heavy Metal Ions in Water. *J. Electroanal. Chem.* **2017**, *788*, 91–98.

(8) Reverté, L.; Prieto-Simón, B.; Campàs, M. New Advances in Electrochemical Biosensors for the Detection of Toxins: Nanomaterials, Magnetic Beads and Microfluidics Systems. A Review. *Anal. Chim. Acta* **2016**, *908*, 8–21.

(9) Wu, S.; Zhao, Q.; Zhou, L.; Zhang, Z. Stripping Analysis of Trace Arsenic Based on the MnOx/AuNPs Composite Film Modified Electrode in Alkaline Media. *Electroanalysis* **2014**, *26* (8), 1840–1849.

(10) Gao, C.; Yu, X.-Y.; Xiong, S.-Q.; Liu, J.-H.; Huang, X.-J. Electrochemical Detection of Arsenic(III) Completely Free from Noble Metal: Fe_3O_4 Microspheres-Room Temperature Ionic Liquid Composite Showing Better Performance than Gold. *Anal. Chem.* **2013**, *85* (5), 2673–2680.

(11) Yang, M.; Chen, X.; Jiang, T. J.; Guo, Z.; Liu, J. H.; Huang, X. J. Electrochemical Detection of Trace Arsenic(III) by Nanocomposite of Nanorod-Like α-MnO_2 Decorated with ∼5 Nm Au Nanoparticles: Considering the Change of Arsenic Speciation. *Anal. Chem.* **2016**, *88* (19), 9720–9728.

(12) Wei, Y.; Yang, R.; Zhang, Y.-X.; Wang, L.; Liu, J.-H.; Huang, X.-J. High Adsorptive γ-AlOOH(Boehmite)@SiO_2/Fe_3O_4 Porous Magnetic Microspheres for Detection of Toxic Metal Ions in Drinking Water. *Chem. Commun.* **2011**, *47* (39), 11062–11064.

(13) Wei, Y.; Gao, C.; Meng, F.-L.; Li, H.-H.; Wang, L.; Liu, J.-H.; Huang, X.-J. SnO_2/Reduced Graphene Oxide Nanocomposite for the Simultaneous Electrochemical Detection of Cadmium(II), Lead(II), Copper(II), and Mercury(II): An Interesting Favorable Mutual Interference. *J. Phys. Chem. C* **2012**, *116* (1), 1034–1041.

(14) Wu, S.; He, Q.; Tan, C.; Wang, Y.; Zhang, H. Graphene-Based Electrochemical Sensors. *Small* **2013**, *9* (8), 1160–1172.

(15) Zuo, Y.; Xu, J.; Zhu, X.; Duan, X.; Lu, L.; Yu, Y. Graphene-Derived Nanomaterials as

Recognition Elements for Electrochemical Determination of Heavy Metal Ions: A Review. *Microchim. Acta* **2019**, *186* (3), 171.

(16) Xu, J.; Wang, Y.; Hu, S. Nanocomposites of Graphene and Graphene Oxides: Synthesis, Molecular Functionalization and Application in Electrochemical Sensors and Biosensors. A Review. *Microchim. Acta* **2017**, *184* (1), 1–44.

(17) Ramesha, G. K.; Sampath, S. In-Situ Formation of Graphene–Lead Oxide Composite and Its Use in Trace Arsenic Detection. *Sensors Actuators B Chem.* **2011**, *160* (1), 306–311.

(18) Devi, P.; Bansod, B.; Kaur, M.; Bagchi, S.; Nayak, M. K. Co-Electrodeposited RGO/MnO_2 Nanohybrid for Arsenite Detection in Water by Stripping Voltammetry. *Sensors Actuators, B Chem.* **2016**, *237*, 652–659.

(19) Devi, P.; Sharma, C.; Kumar, P.; Kumar, M.; Bansod, B. K. S.; Nayak, M. K.; Singla, M. L. Selective Electrochemical Sensing for Arsenite Using RGO/Fe_3O_4 Nanocomposites. *J. Hazard. Mater.* **2017**, *322*, 85–94.

(20) Altundoğan, H. S.; Altundoğan, S.; Tümen, F.; Bildik, M. Arsenic Adsorption from Aqueous Solutions by Activated Red Mud. *Waste Manag.* **2002**, *22* (3), 357–363.

(21) Bhatnagar, A.; Vilar, V. J. P.; Botelho, C. M. S.; Boaventura, R. A. R. A Review of the Use of Red Mud as Adsorbent for the Removal of Toxic Pollutants from Water and Wastewater. *Environ. Technol.* **2011**, *32* (3), 231–249.

(22) Abdolhosseinzadeh, S.; Asgharzadeh, H.; Kim, H. S. Fast and Fully-Scalable Synthesis of Reduced Graphene Oxide. *Sci. Rep.* **2015**, *5*, 10160.

(23) Bastwros, M.; Kim, G.-Y.; Zhu, C.; Zhang, K.; Wang, S.; Tang, X.; Wang, X. Effect of Ball Milling on Graphene Reinforced Al6061 Composite Fabricated by Semi-Solid Sintering. *Compos. Part B Eng.* **2014**, *60*, 111–118.

(24) Granger, M. C.; Witek, M.; Xu, J.; Wang, J.; Hupert, M.; Hanks, A.; Koppang, M. D.; Butler, J. E.; Lucazeau, G.; Mermoux, M.; Strojek, J.W.; Swain, M. G. Standard Electrochemical Behavior of High-Quality, Boron-Doped Polycrystalline Diamond Thin-Film Electrodes. *Anal. Chem.* **2000**, *72* (16), 3793–3804.

(25) Benedito da Silva, O.; Machado, S. A. S. Evaluation of the Detection and Quantification Limits in Electroanalysis Using Two Popular Methods: Application in the Case Study of Paraquat Determination. *Anal. Methods* **2012**, *4* (8), 2348–2354.

(26) Gumpu, M. B.; Veerapandian, M.; Krishnan, U. M.; Rayappan, J. B. B. Simultaneous

Electrochemical Detection of Cd(II), Pb(II), As(III) and Hg(II) Ions Using Ruthenium(II)-Textured Graphene Oxide Nanocomposite. *Talanta* **2017**, *162*, 574–582.

(27) Salimi, A.; Mamkhezri, H.; Hallaj, R.; Soltanian, S. Electrochemical Detection of Trace Amount of Arsenic(III) at Glassy Carbon Electrode Modified with Cobalt Oxide Nanoparticles. *Sensors Actuators B Chem.* **2008**, *129* (1), 246–254.

(28) Gupta, R.; Gamare, J. S.; Pandey, A. K.; Tyagi, D.; Kamat, J. V. Highly Sensitive Detection of Arsenite Based on Its Affinity toward Ruthenium Nanoparticles Decorated on Glassy Carbon Electrode. *Anal. Chem.* **2016**, *88* (4), 2459–2465.

(29) Gu, T.; Bu, L.; Huang, Z.; Liu, Y.; Tang, Z.; Liu, Y.; Huang, S.; Xie, Q.; Yao, S.; Tu, X.; Luo, X.; Luo, S. Dual-Signal Anodic Stripping Voltammetric Determination of Trace Arsenic(III) at a Glassy Carbon Electrode Modified with Internal-Electrolysis Deposited Gold Nanoparticles. *Electrochem. commun.* **2013**, *33*, 43–46.

(30) Zhang, Q.-X.; Yin, L.-B. Electrochemical Performance of Heterostructured Au–Pd Bimetallic Nanoparticles toward As(III) Aqueous Media. *Electrochem. commun.* **2012**, *22*, 57–60.

(31) Moghimi, N.; Mohapatra, M.; Leung, K. T. Bimetallic Nanoparticles for Arsenic Detection. *Anal. Chem.* **2015**, *87* (11), 5546–5552.

(32) Zhou, S. F.; Han, X. J.; Fan, H. L.; Zhang, Q. X.; Liu, Y. Q. Electrochemical Detection of As(III) through Mesoporous MnFe2O4 Nanocrystal Clusters by Square Wave Stripping Voltammetry. *Electrochim. Acta* **2015**, *174*, 1160–1166.

(33) Li, S. S.; Zhou, W. Y.; Jiang, M.; Guo, Z.; Liu, J. H.; Zhang, L.; Huang, X. J. Surface Fe(II)/Fe(III) Cycle Promoted Ultra-Highly Sensitive Electrochemical Sensing of Arsenic(III) with Dumbbell-Like Au/Fe_3O_4 Nanoparticles. *Anal. Chem.* **2018**, *90* (7), 4569–4577.

(34) Zhang, Z.-J.; Wang, Y.-X.; Chou, S.-L.; Li, H.-J.; Liu, H.-K.; Wang, J.-Z. Rapid Synthesis of α-Fe2O3/RGO Nanocomposites by Microwave Autoclave as Superior Anodes for Sodium-Ion Batteries. *J. Power Sources* **2015**, *280*, 107–113.

(35) Bhattacharya, G.; Fishlock, S. J.; Roy, J. S.; Pritam, A.; Banerjee, D.; Deshmukh, S.; Ghosh, S.; McLaughlin, J. A.; Roy, S. S. Effective Utilization of Waste Red Mud for High Performance Supercapacitor Electrodes. *Glob. Challenges* **2019**, *3* (2), 1800066.

(36) Zhang, J.; Yang, H.; Shen, G.; Cheng, P.; Zhang, J.; Guo, S. Reduction of Graphene Oxide

Vial-Ascorbic Acid. *Chem. Commun.* **2010**, *46* (7), 1112–1114.

(37) Alp, A.; Goral, M. S. The Influence of Soda Additive on the Thermal Properties of Red Mud. *J. Therm. Anal. Calorim.* **2003**, *73* (1), 201–207.

(38) Scheibe, B.; Mrówczyński, R.; Michalak, N.; Załęski, K.; Matczak, M.; Kempiński, M.; Pietralik, Z.; Lewandowski, M.; Jurga, S.; Stobiecki, F. Anchoring Fe_3O_4 Nanoparticles in a Reduced Graphene Oxide Aerogel Matrix via Polydopamine Coating. *Beilstein J. Nanotechnol.* **2018**, *9*, 591–601.

Table of Contents image

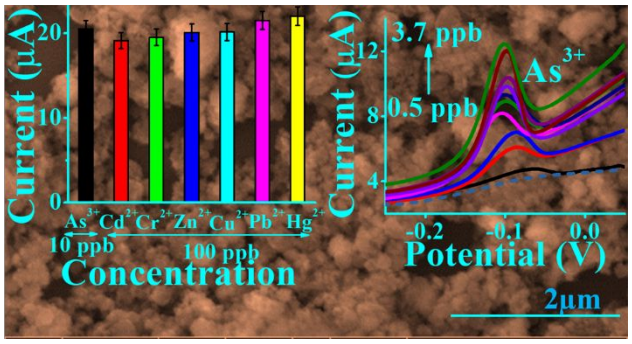

Selective electrochemical detection of As^{3+} ions using red mud-rGO nanocomposite.